Chinese Chemical Letters 35 (2024) 109060

Contents lists available at ScienceDirect

Chinese Chemical Letters

journal homepage: www.elsevier.com/locate/cclet

Engineered exosome hybrid copper nanoscale antibiotics facilitate simultaneous self-assembly imaging and elimination of intracellular multidrug-resistant superbugs

Zengchao Guo[a], Weiwei Liu[a], Tengfei Liu[a], Jinpeng Wang[a], Hui Jiang[a], Xiaohui Liu[a,*], Yossi Weizmann[b,*], Xuemei Wang[a,*]

[a] State Key Laboratory of Digital Medical Engineering, School of Biological Science and Medical Engineering, Southeast University, Nanjing 210096, China
[b] Department of Chemistry, Ben-Gurion University of the Negev, Beer-Sheva 8410501, Israel

ARTICLE INFO

Article history:
Received 6 July 2023
Revised 1 September 2023
Accepted 7 September 2023
Available online 10 September 2023

Keywords:
In situ self-assembled
Exosome
Antibacterial agents
Bioimaging
Intracellular infection

ABSTRACT

With the increasing emergence of bacterial infections, especially multidrug-resistant (MDR) bacteria, poses an urgent threat. This study demonstrated a novel multifunctional nanotheranostics platform developed by the strategic integration of both *in-situ* bio-assembly imaging and target bacteria inactivation. Through the introduction of copper ions into bacteria, the Cu^{2+} could spontaneously bio-self-assembled into a multifunctional copper nanoclusters (NCs) which efficiently enhanced epigallocatechin gallate (EGCG) uptake into bacteria. While visualizing the bacteria, the developed theranostic nanoplatform exhibited highly efficient disinfection activities with negligible side effects as reflected by higher cell viability and insignificant hemolytic effects. Furthermore, the exosomal formulation of EGCG integrated with Cu^{2+} showed an increased intracellular antibacterial activity, which could eliminate most of the methicillin-resistant *Staphylococcus aureus* (MRSA) phagocytosed by macrophages, guide macrophages toward M2-like phenotype polarization and alleviate inflammation, without exhibiting obvious cytotoxicity on host RAW264.7. The regimen could be viewed as an effective strategy for the sterilization of intractable bacterial infections.

Bacteria have historically been identified as “invisible killers” posing a major health concerns [1]. Since the invention of penicillin [2], antibiotics have been widely used as effective measures against bacterial infections. Nevertheless, the continuous abuse of antibiotics, has resulted in gene mutation and thus the birth of multidrug-resistant (MDR) strains, which have narrowed the conventional anti-bacterial spectrum of antibiotics [3,4]. The increase in drug-resistant bacteria is outpacing the number of antibiotics approved to treat them [5]. Studies have demonstrated that in the 21st century, there is an average of 1–2 new antibiotics approved by the Food and Drug Administration (FDA) annually [6]. Reports have revealed that if no new antibacterial strategies are found by 2050, millions of people could die from MDR bacterial infections [7].

Currently, natural antibacterial compounds, have been shown to be a promising anti-bacterial option that avoid over-use and drug resistance of antibiotics [8]. Green tea (*Camellia sinensis*, Theaceae) is one of the most popular beverages containing polyphenols. Numerous reports have shown that it possesses powerful medical values [9]. Epigallocatechin gallate (EGCG), a major polyphenol bioactive ingredient has gained much attention in recent years [10,11], categorized as “generally recognized as safe” (GRAS) by the FDA. It has good biocompatibility and linked to a variety of health benefit such as anti-inflammatory, antiviral, antitumor, and effectively promoting wound healing/tissue repair [12–14]. It also possesses great anti-infective potential as it has a wide range of bactericidal activity and inhibits biofilm formation [15,16]. However, EGCG has several drawbacks which limit its bioavailability and biological activities, including poor solubility, weak stability, short half-life and rapid metabolism [17]. That can be dealt with using a suitable vehicle that delivery EGCG to the action site and effective protects against biodegradation or *in vivo* degradation [18].

Bacteria such as *E. coli*, methicillin-resistant *Staphylococcus aureus* (MRSA) and *S. aureus* have the ability to invade and survive in host cells, particularly macrophages, where they multiply into a reservoir, evading the immune response and establishing persistent infections [19]. Bacterial localization can disrupt the normal

* Corresponding authors.
E-mail addresses: 101013182@seu.edu.cn (X. Liu), yweizmann@bgu.ac.il (Y. Weizmann), xuewang@seu.edu.cn (X. Wang).

https://doi.org/10.1016/j.cclet.2023.109060
1001-8417/

functioning of macrophages and create a preferential niche, making it harder for the host defense mechanisms and drugs to eliminate them [20]. Dealing with intracellular bacterial infections remains a significant challenge as most of the current antibiotics such as gentamycin, macrolides and β-lactams are gradually becoming inefficient against intracellular bacterial due to no or only limited accumulation in eukaryotic cells, or because of poor intracellular retention [21,22]. Statistically, more than two-thirds of prescribed antibiotics are not effective in treating intracellular bacteria [23]. To overcome the existing limitations, extensive studies have shown that the nanometer-sized delivery systems can effective encapsulate, protect and release bioactive substances, such as drugs and nutrients [24]. The exploration of intracellular vesicles in recent years have become a hotspot of research. Exosomes are nanoscale microvesicles of cellular origin, with a diameter ranging of 30–200 nm that naturally released by practically all types of cells [25,26]. As natural carriers that package various substances, they specialized in long-distance intercellular communications with a stable and long circulation times [27,28]. The application of exosomes in an ideal system as potential carriers for various dispositions, such as cancer, inflammation, or tissue injury is on a rise [29–33].

The endogenous origin of exosomes endows them multiple advantages with nontoxic, low-immunogenicity, able to cross biological barriers, stability and a long half-life circulation ability under physiological conditions [34–36]. In addition, the homing ability and specific cell tropism of exosomes has gained attention and are postulated to have excellent targeting effects that do not require postfabrication modifications compared to synthetic drug carriers [37–39]. Consequently, exosomes could serve as an "invisible shield" for incorporated bioactive molecules with substantial cargo-loading and protective abilities, diminishing clearance due to the immune privileged status and maximize transportation of therapeutic drugs to designated locations.

Copper (Cu) is an essential transition metal element in the body. Copper, silver and zinc are the most representative antibacterial metal materials, which have the advantages of high sterilization efficiency, broad antibacterial spectrum and good stability [40,41]. Studies have shown that in the presence of the Cu^{2+}, tea catechins exhibited apparent pro-oxidative properties that induced DNA cleavage, accelerated the peroxidation of fatty acid, and enhanced bactericidal performance [42,43]. The bacterial microenvironment has emerged as a suitable target for specific recognition and treatment of relatively infectious diseases because of its differences compared to normal tissues [44], such as hypoxia, elevated glutathione (GSH)-glutathione oxidized (GSSG) and nicotinamide adenine dinucleotide phosphate ($NADP^+$)-reduced nicotinamide adenine dinucleotide phosphate (NADPH) [45,46], as well as the ubiquitous reducing power of bacteria [47,48]. The formation of nanoparticles inside the bacteria was likely involved in bacterial defense mechanisms against metallic ions, which included bioaccumulation, biomineralization, and biosorption [49,50]. Here, a simplified and efficient method was constructed for bio-reducing and self-assembled to metal nanocomplexes inside bacteria for simultaneous bioimaging and theranostics by introducing Cu^{2+} that leverage the distinct microenvironment of bacteria and increase the uptake of EGCG into bacteria. Furthermore, we investigated the possibility that using exosomes as delivery agents to treat intracellular infection and revealed robust therapeutic efficacy in an *in vitro* infection model using macrophages and MRSA. This offers novel understanding into merging bioimaging technology with effective antibacterial abilities, and shows promise of developing a challenging clinical application strategy with a multimodal strategy.

The imaging performance was initially assessed by confocal microscopy for MRSA visualization with different treatments. Cu^{2+} with/without EGCG was co-cultured with bacterial for 3 h, the control group was given phosphate buffer saline (PBS). Fig. 1A demonstrated that no fluorescence was detected both in the control and EGCG group. On the contrary, the presence of Cu^{2+} resulted in bright fluorescence in the intracellular region which may be due to *in situ* synthesis of fluorescent-emitting copper nanoclusters in the presence of Cu^{2+} because of the unique microenvironment of bacteria compared to normal tissues [44]. At the same time, we also observed the intensity of the Cu group slightly weaker than that of the EGCG-Cu group after introducing EGCG. This could be due to the fluorescence intensification of EGCG as a ligand to keep the formed NCs stable, and EGCG also contributes to the reduction of Cu^{2+} by gaining an electron pair around "EGCG's hydroxyl groups" oxygen. Furthermore, the relative intensity of each group was quantitatively compared to show the difference in fluorescence intensity more clearly (Fig. 1B). The reconstructed 3-dimensional of EGCG-Cu group fluorescence image was shown in Fig. 1C. It demonstrated the successful *in situ* synthesis of fluorescent copper nanoclusters (EGCG-Cu NCs) in bacteria when incubated with Cu^{2+} solution, followed by EGCG for precise bioimaging and treatment. By contrast, no fluorescent EGCG-Cu NCs were formed in the control group. This demonstrated that EGCG-Cu NCs could be synthesis by bacteria and used as a nanoscale biomarker for bacteria detection.

In order to analyze the antibacterial property against bacteria, the activity of EGCG-Cu NCs was studied by measuring the MICs. It showed that EGCG and Cu^{2+} presented concentration- and time-dependent antibacterial behavior (Fig. S1 in Supporting information). Specifically, *S. aureus* after various treatments were diluted and coated onto agar plates. As illustrated in Fig. 1E, with the increase of EGCG concentration under Cu^{2+} concentration of 8 μg/mL, antibacterial properties were presented in the number of bacterial colonies. We further evaluated the antibacterial capability of the EGCG-Cu against MRSA. To our knowledge, MRSA is typically resistant to more than 10 antibiotics [51]. By contrast, EGCG can inhibit the multiplication of MRSA with the minimal inhibitory concentration (MIC) of 32 μg/mL under Cu^{2+} concentration of 16 μg/mL (Figs. 1D and E). Bacterial biofilm is an intricate matrix composed of bacteria, proteins, and polysaccharides that can foster persistent infections and increase resistance to drugs, rendering them notoriously difficult to eradicate [52,53]. Hence, we carried out the crystal violet staining and imaging analysis to detect the inhibition properties for biofilm. As visualized in Figs. S2A and S3 (Supporting information), the EGCG-Cu group was able to dramatically reduce the formation of MRSA biofilms and barely any cellular clumps were detected. Quantification of biofilm biomass of MRSA after different treatments also showed the same trend (Fig. S2B in Supporting information), verifying that EGCG-Cu had the highest ability against biofilm. The biofilm extracellular polymeric substances (EPS) play a crucial role in biofilms formation [54]. Therefore, the effect on the secretion of polysaccharides and proteins, the primary components of EPS, was studied. As shown in Figs. S2C and D (Supporting information), the extracellular protein and polysaccharide formation of the group treated with EGCG-Cu was the lowest compared to other treatments, further confirmed the inhibition effect of EGCG-Cu on bacterial biofilm formation. The results clearly confirmed the excellent antibacterial effect of the antibacterial agent.

The EGCG-Cu NCs have been extracted from the MRSA for further characterization. It is reported that ultrasmall metal NCs possess excellent physicochemical properties, and show diversified applications potential in sensing, imaging, and biomedicine [55,56]. As illustrated in Fig. S4A (Supporting information), transmission electron microscope (TEM) image revealed that most of the EGCG-Cu NCs were mainly spherical and did not significantly aggregate at room temperature. Furthermore, these NCs were characterized by dynamic light scattering (DLS). The sample did not have

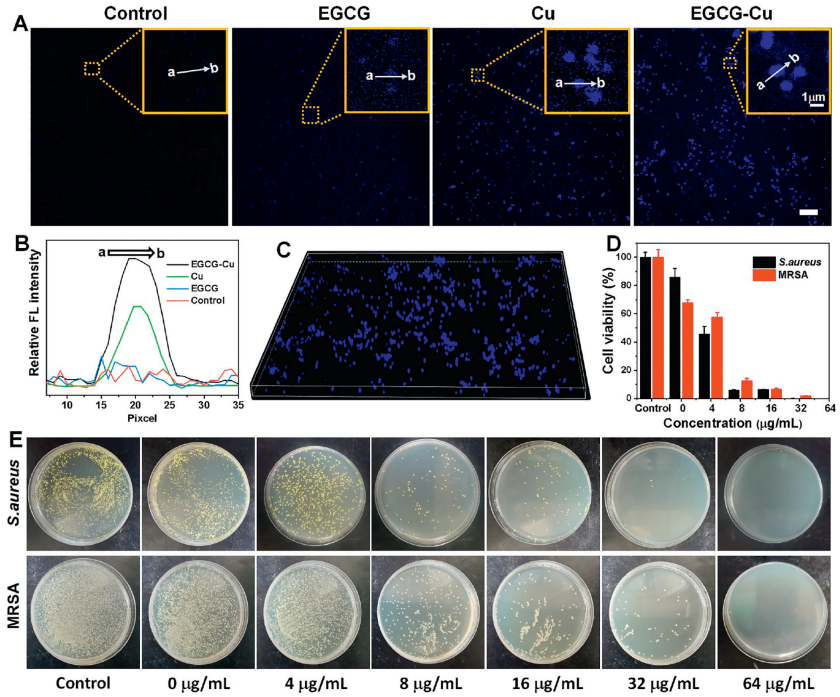

Fig. 1. Bioimaging studies of relevant bacterial cells. (A) Laser confocal fluorescence imaging of MRSA with different treatment. Scale bar: 10 μm. (B) Quantitative analysis of relative fluorescence intensity as shown in A. (C) The image shows the reconstructed 3-dimensional of EGCG-Cu group images. (E) *S. aureus* and MRSA photographs of the agar plates and (D) the corresponding statistical histogram of bacterial colonies after different treatments as indicated. Error bars: mean ± standard deviation (SD) ($n = 3$).

multiple peaks with a distribution peak at *ca.* 3.52 nm, and the diameter distribution was found to be very narrow, further indicated that the particle size was uniform (Fig. S4B in Supporting information). At the same time, as seen from Fig. S4C (Supporting information), X-ray photoelectron spectroscopy (XPS) was employed to characterized the valence state of Cu in the NCs, where the prominent peaks appeared at 952.7 and 932.8 eV were attributed to Cu $2p_{1/2}$ and Cu $2p_{3/2}$, which were characteristic peaks due to Cu(0). In addition, it is worth mentioning that the peak due to Cu(I) occurs at 0.1 eV apart from Cu(0), its presence cannot be readily excluded [57]. As shown in Fig. S5A (Supporting information), it was discovered that abnormal Cu could be readily detected in the EDS spectrum of NCs, while no other metallic elemental impurities were observed. In addition, Fourier transforms infrared spectra (FTIR) was employed to examine the interaction between Cu^{2+} and EGCG in the self-assembly EGCG-Cu NCs (Fig. S4D in Supporting information). The FTIR showed that the differences between the two spectra could be presented, indicating that the bands at 3421, 1717 and 1103 cm^{-1}, which were attributed to O-H stretching vibration, C=C and C-O bonds in the EGCG were shifted slightly after mixing with Cu. This suggested that there was an interaction between the functional groups of EGCG and Cu^{2+}. We can conclude that the detected Cu were derived from the complexes added, and further proved that Cu NCs were formed successfully.

To clarify the effect of EGCG-Cu on bacterial condition, the morphological changes of MRSA after various treatments were studied. As demonstrated in Fig. S6A (Supporting information), untreated MRSA showed typical shapes, even cell surfaces, and maintained intact morphology. Besides, minor morphological alterations and a mild degree of distortion on the exterior of some bacteria were discovered in Cu- and EGCG-treated groups. In comparison, the form of the MRSA after being treated with EGCG-Cu changed drastically and showed signs of clear damage. Numerous additional indentations were noticed on the cellular surfaces, affirming the robust efficacy of EGCG-Cu for causing harm to bacteria. Furthermore, fluorescence pictures of calcein acetoxymethyl ester/propidium Iodide (calcein-AM/PI) double staining demonstrated that only bright green fluorescence and no visible red fluorescence were present in control group (Figs. S6B and C in Supporting information). However, the bacteria exposure to EGCG-Cu emitted only red fluorescence, proved that the MRSA were completely destroyed and the bacterial cellular membranes were incomplete/flawed, thus allowing PI to enter the bacterial cells and bind to nucleic acids.

The cytoplasmic membrane acts as a structural unit and undoubtedly is the target of many antibacterial agents. The bacterial membranes would become breached when encountering antibacterial drugs [58,59]. The membrane rupture leads to the release of intracellular constituents that can be detected in the surrounding environment. Thus, the release level of intracellular constituents is a hallmark of membrane integrity. The degree of protein leakage can be used as a response to the extent of cell damage [60]. As shown in Fig. S6D (Supporting information), the release of intracellular components was altered after exposure to different groups. The amount of protein released from the bacteria release fluid exposure to EGCG-Cu was higher than other groups, indicated a more serious disruption. In general, these results confirmed that EGCG-Cu could strongly interact with the pathogenic cell membranes and further lead to the flow of a large number of intracellular proteins, which ultimately lead to the death of such superbugs by cell damage.

Catechins have been reported to promote oxidative cleavage of DNA in the presence of Cu^{2+} [42,43]. To examine this regard, we extracted and characterized the bacterial genomic DNA through electrophoretic analysis after different treatments. As presented in Fig. S7B (Supporting information), the EGCG-Cu group exhibited significant smearing on its DNA band compared with other groups, indicated the presence of shorter DNA fragments and the most severe DNA damage occurred.

Based on the relationship between the bactericidal effect and intracellular redox levels, the reactive oxygen species (ROS) in MRSA were also evaluated to affirm the intracellular level

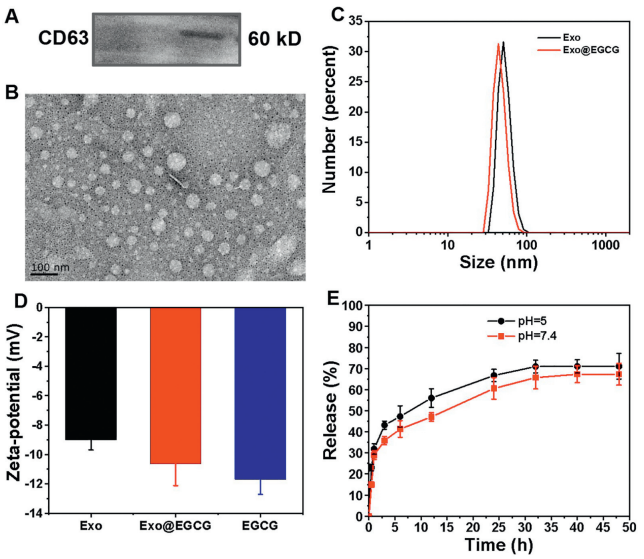

Fig. 2. Preparation and characterization of purified exosomes and exosome-based hybrid nanostructures. (A) Western blot of RAW264.7 cell-derived exosomes using anti-CD63 antibody. (B) Representative micrographs of exosomes as analyzed by TEM. (C) Size distribution and (D) zeta potential of exosomes before and after EGCG loading. (E) Time course of EGCG release from pre-loaded exosomes at pH 5 and 7.4 was evaluated. Error bars: mean ± SD ($n = 3$).

of ROS among the different treatment groups [61,62]. 2′7′-Dichlorofluorescein diacetate (DCF-DA) can be hydrolyzed by the intracellular esterases to produce DCFH which can be oxidized by ROS to form fluorescent DCF. Results of the ROS generation analysis (Figs. S6E and F in Supporting information) showed that EGCG-Cu treatment group had higher levels of ROS compared to the other groups. Similarly, flow cytometry analysis also showed increased ROS level in MRSA after treated with EGCG-Cu (Fig. S7A in Supporting information). Lipid peroxidation (LPD) can be used as a biomarker to study the role of ROS production. As illustrated in Fig. S7C (Supporting information), EGCG-Cu group presented a high LPD level compared to other groups, implied more ROS were produced, which was consistent with our ROS analysis results. This conclusion further confirmed that the EGCG-Cu group had the most severe bacterial cell membrane damage.

To minimize the effects on the immune system, and avoid potential long-term risks, but also considering the production of exosomes, macrophages (RAW264.7) were chosen as the parent cells. In this study, bare exosomes were isolated from the supernatants of RAW264.7 through differential ultracentrifugation steps. The prepared exosome (Exo) was used as a drug delivery vehicle and loaded with EGCG (Exo@EGCG) as an antibacterial agent. Exosome-associated proteins, such as CD63 (Fig. 2A), were identified by western blotting analysis of RAW264.7 cell-derived exosomes. The electron micrograph in Fig. 2B show typical morphology of spherical empty exosomes nanostructure and they are well dispersed. DLS revealed a relatively narrow size intensity distribution, with a mean particle diameter of objective product was 52.90 ± 9.92 nm (Fig. 2C). Furthermore, the surface charges of exosomes were performed using zeta potential, and the average zeta potential was −9.01 ± 0.694 mV (Fig. 2D). We subsequently acquired EGCG-loaded exosomes (Exo@EGCG) using a simple mechanical extrusion process, followed by centrifugation to eliminate the free drug.

The whole-size distribution showed a slight leftward shift upon loading with EGCG, and the size of loaded exosomes at peak concentration decreased to 45.97 nm (Fig. 2C). In addition, after loading of EGCG, the measured zeta potential of prepared nanoformulations decreased from −9.01 mV to −10.62 mV (Fig. 2D). It was possible that the slightly altered diameter and potential could be attributed to the extrusion process and cargo encapsulation. It is well established that the anionic phospholipid phosphatidylserine is abundantly present on membranes and plays a role in the surface charge of individual cellular membranes. Taken together, the loading process had no significant effect on the zeta potential of the original exosomes, indicating no major changes to the lipid composition of exosomal membranes and still maintained the properties of original exosomes. The drug loading capacity (DL) of EGCG in exosomes was determined using the standard of "absorbance value-concentration" (Fig. S8 in Supporting information), approximately 34.56% of EGCG were loaded into the exosomes. Moreover, the release kinetics of EGCG from pre-loaded exosomes was carried out in PBS (pH 7.4 and 5) at predetermined time intervals by ultraviolet–visible (UV–vis) spectrophotometry. As displayed in Fig. 2E, EGCG was continuously released in a time-dependent manner, regardless of the release media, with a prolonged and sustained release over 48 h. The release behavior of EGCG was similar in both media preparations, suggesting a minimal influence of pH on the release profile. The slow release of nanoformulations is favorable for drug administration.

The prerequisite for exosomal formulations to function is based on the effective uptake of the drug payload by target cells, which was essential for the efficacy of exosomal formulations. For this purpose, we investigated the cellular uptake efficiency of the Dio-labeled exosomes formulation by RAW264.7 cells and investigated whether manipulations with exosomes impact their delivery to target cells. As shown in Fig. S10A, the fluorescence intensity increased in a time-dependent manner revealing that the exosomes labeled by DiO were efficiently migrated to RAW264.7 macrophage over time, and they were principally around the macrophage nucleus. To better show the uptake, partial enlargements are presented as shown in Fig. S10B. Interestingly, the cellular uptake profile showed similar intracellular fluorescence after treated with either exosomes or Exo@EGCG hybrids, which suggested that the drug payload did not affect the internalization of these exosomes (Fig. S9 in Supporting information).

For any antibacterial formulations, estimating the potential adverse effect is crucial. To examine the preliminary biocompatibility of Cu^{2+} and EGCG, we conducted a cell counting (CCK-8) test by using L02 and RAW264.7 as mammalian cells models. It showed that Cu^{2+} and EGCG had concentration-dependent cytotoxicity as displayed in Fig. S11 (Supporting information) and Figs. 3A and B. And the Exo@EGCG-Cu showed negligible toxicity to both cells even at a higher concentration of 256 μg/mL of EGCG. Additionally, hemolytic behavior was further analyzed by treating erythrocytes and the hemolysis rate of erythrocytes remained below 20% at doses up to 64 μg/mL of either Cu^{2+} or EGCG solutions, which was much higher than the MIC for bacteria.

The intracellular antibacterial property was further assessed using a co-culture model of MRSA and RAW264.7, a conventional mononuclear phagocyte system infection model [63]. We first studied the distribution of MRSA in RAW264.7 after different treatments to investigate the bacteria targeting effect of NCs. As shown in Fig. 3E, EGCG-Cu and Exo@EGCG-Cu groups all exhibited a specific fluorescence in the cytoplasm of macrophages, which confirmed the successful bio-assembly of Cu NCs based on target infections. Additionally, another remarkable feature was that the uninfected cells showed little or no fluorescence under identical experimental conditions, as displayed in Fig. S12 (Supporting information), which was attributed to no NCs formation and the bio-assembly of NCs only occurred within bacteria. The count of MRSA colonies confirmed the effective antibacterial properties of Exo@EGCG-Cu against MRSA inside the RAW264.7 cells. Compared to the other groups, the amount of intracellular MRSA dramatically

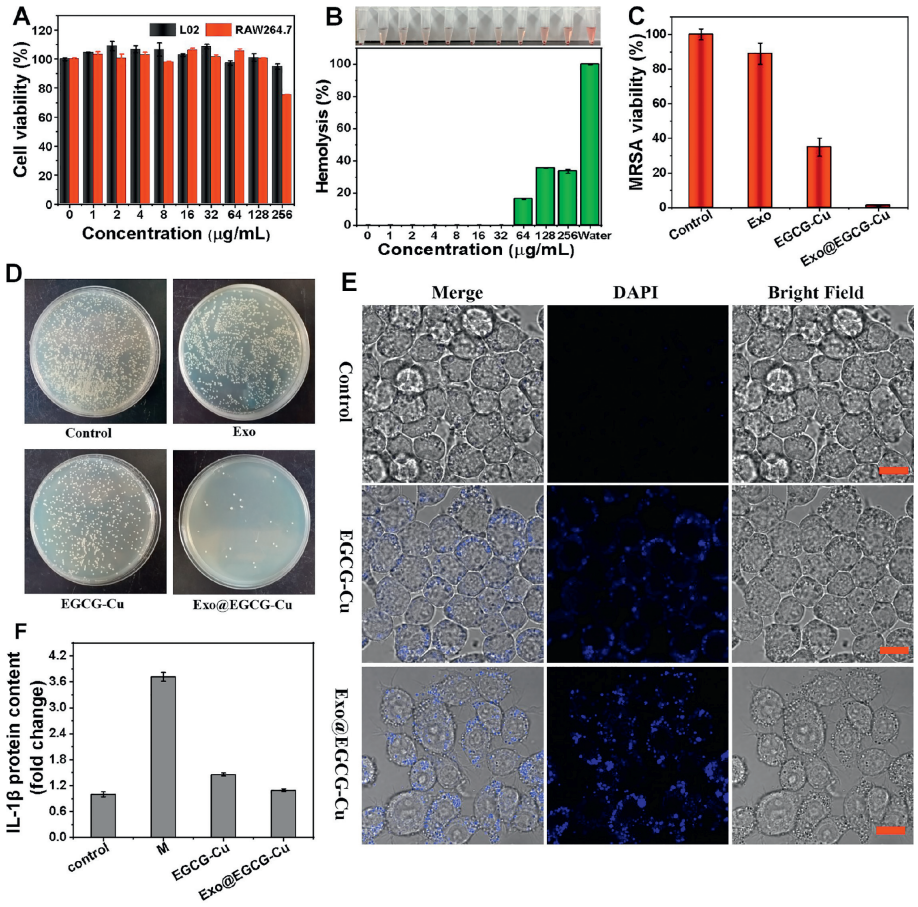

Fig. 3. Survival rates of cells (A) and hemolysis of red blood cells (B) in the presence of copper salt (16 μg/mL) with various concentrations of Exo@EGCG. (D) Photographs and (C) corresponding statistics of MRSA colonies formed on LB agar plates after co-culture experiments of MRSA and RAW264.7 macrophages. (E) Confocal laser scanning microscope (CLSM) images of MRSA-infected RAW264.7 macrophages after different treatments. Scale bar: 10 μm. DAPI, 4′,6-diamidino-2-phenylindole. (F) The expression level of inflammatory factor IL-β after different cell treatments. Error bars: mean ± SD ($n = 3$).

reduced in the Exo@EGCG-Cu group (Figs. 3C and D). Furthermore, we discovered that the amount of RAW264.7 did not decrease after treatment, further verified the good biocompatibility to macrophage cells (Fig. S13A in Supporting information).

For bacterial-associated infections, the long-term existence of bacteria lead to a persistent inflammatory state and seriously disturbs the normal repair process [64]. Next, to examine the effect of Exo@EGCG-Cu on the inflammatory response of RAW264.7 after the treatment of intracellular infections, the essential inflammatory factor interlenkin-1β (IL-1β) was tested by enzyme linked immunosorbent assay (ELISA). As shown in Fig. 3F, MRSA infection could dramatically stimulate the activation of IL-1β in RAW264.7. After treatment, IL-1β secreted by RAW264.7 was sharply down-regulated and ameliorated the inflammation reaction. Additionally, we found that uninfected macrophages did not show a visible inflammatory level under identical experimental conditions (Fig. S13B in Supporting information). Macrophages perform critical functions in regulating inflammation through polarization [65,66]. CD86 and CD206 are widely used as markers for proinflammatory M1 macrophages and anti-inflammatory M2 macrophages, respectively [67,68]. Hence, the influence on macrophage polarization *in vitro* was preliminarily assessed by flow cytometry. As displayed in Fig. S14 (Supporting information), the numbers of M1-like macrophages and M2-like macrophages did not differ significantly between the control and Exo groups. Nevertheless, the proportion of M2-like macrophages increases and M1-like macrophages decreases in the EGCG-Cu group. Exo@EGCG-Cu group could further increase the proportion of M2-like macrophages and reduce the proportion of M1-like macrophages. These data demonstrate that Exo@EGCG-Cu could significantly eliminate MRSA inside the RAW264.7 with inhibit inflammation, but with no harm to the cells.

Subsequently, *in vivo* healing ability was assessed in the bacteria-infected wound skin of mice. All *in vivo* experiments were performed under relevant protocols approved by the Animal Care Committee of Southeast University. The representative images of wound closure at given time points were displayed in Fig. S15 (Supporting information). As time went by, the wounds in all treated groups became smaller. Specifically, the relative wound area decreased greatly after Exo@EGCG-Cu treatment and almost disappeared on day 8. As a comparison, it exhibited limited wound healing effects for other groups. The surface area in the wound site was calculated to further evaluate the bactericidal ability *in vivo* (Fig. S15B). The results showed that the surface area after Exo@EGCG-Cu treatment was remarkably decreased to 16% on day 6, while the surface area in other groups remained above 35%. In addition, as shown in Fig. S15C, the body weight curves indicated that there was no evident side effect on mice growth. Thus, the above results preliminarily verified effective antibacterial activity that accelerated the wound closure after Exo@EGCG-Cu treatment.

In this study, we have explored a facile multimode antimicrobial mode for labeling and inactivation of bacterial by introducing Cu^{2+} and then a combination with EGCG. The interdependent and synergistic effects of Cu^{2+} and EGCG enhanced the visualization of bacteria and exhibited highly efficient disinfection activities by inducing severe deformation of the bacterial membrane. Worth

noting is the fact that the developed bactericide could also effectively inhibit the formation of bacteria biofilm thereby preventing the emergence of bacterial resistance. In addition, the exosomal formulation of EGCG integrate with Cu^{2+} showed an increased intracellular antibacterial activity, which could inactivate most of MRSA phagocytosed by RAW264.7, and no obvious cytotoxicity was found on host RAW264.7. In summary, results from this study brought forth the possibility of providing a novel, inexpensive and effective approach to fight against infections and bacteria-induced diseases.

Declaration of competing interest

The authors declare that they have no known competing financial interests or personal relationships that could have appeared to influence the work reported in this paper.

Acknowledgments

This work was supported by the National Natural Science Foundation of China (Nos. 82061148012, 82027806, 92061121, 91753106), the National Key Research and Development Program of China (No. 2017YFA0205300), Primary Research & Development Plan of Jiangsu Province (No. BE2019716) and the ISF-NSFC Joint Research Program (No. 3258/20) to Yossi Weizmann.

Supplementary materials

Supplementary material associated with this article can be found, in the online version, at doi:10.1016/j.cclet.2023.109060.

References

[1] P.A. Rota, M.S. Oberste, S.S. Monroe, et al., Science 300 (2003) 1394–1399.
[2] A. Fleming, Br. J. Exp. Pathol. 10 (1929) 226–236.
[3] Y. Zheng, H. Jiang, X. Wang, Chin. Chem. Lett. 31 (2020) 3183–3189.
[4] J. Bresee, C.M. Bond, R.J. Worthington, et al., J. Am. Chem. Soc. 136 (2014) 5295–5300.
[5] N. Guo, Y. Xia, Y. Duan, et al., Chin. Chem. Lett. 34 (2023) 107542.
[6] A.J. Huh, Y.J. Kwon, J. Control. Release 156 (2011) 128–145.
[7] E.D. Brown, G.D. Wright, Nature 529 (2016) 336–343.
[8] Y. Wang, Y. Yang, Y. Shi, et al., Adv. Mater. 32 (2020) 1904106.
[9] D.W. Tang, S.H. Yu, Y.C. Ho, et al., Food Hydrocolloids 30 (2013) 33–41.
[10] B. Hu, Y. Shen, J. Adamcik, et al., ACS Nano 12 (2018) 3385.
[11] P.M. Seidler, K.A. Murray, D.R. Boyer, et al., Nat. Commun. 13 (2022) 5451.
[12] M. Shin, E. Park, H. Lee, Adv. Funct. Mater. 29 (2019) 1903022.
[13] K. Li, G. Xiao, J.J. Richardson, et al., Adv. Sci. 6 (2019) 1801688.
[14] A. Cano, M. Ettcheto, J.H. Chang, et al., J. Control. Release 301 (2019) 62–75.
[15] J. Zhang, X. Rui, L. Wang, et al., Food Control 42 (2014) 125–131.
[16] C. Knidel, M.F. Pereira, D.H.F. Barcelos, et al., Nat. Prod. Res. 35 (2021) 4643–4647.
[17] W.Z. Dai, C.C. Ruan, Y.M. Zhang, et al., J. Funct. Foods 65 (2020) 103732.
[18] O. Krupkova, S.J. Ferguson, K. Wuertz-Kozak, J. Nutr. Biochem. 37 (2016) 1–12.
[19] M.G. Elnaggar, K. Jiang, H.E. Eldesouky, et al., Biomaterials 262 (2020) 120344.
[20] E. Imbuluzqueta, E. Elizondo, C. Gamazo, et al., Acta Biomater. 7 (2011) 1599–1608.
[21] J.H. Yeom, B. Lee, D. Kim, et al., Biomaterials 104 (2016) 43–51.
[22] F. Pea, Clin. Pharmacokinet. 57 (2018) 177–189.
[23] M.S. Butler, M.A. Blaskovich, M.A. Cooper, J. Antibiot. 66 (2013) 571–591.
[24] J. Liang, H. Yan, X. Wang, et al., Food Chem. 231 (2017) 19–24.
[25] M. Tkach, C. Thery, Cell 164 (2016) 1226–1232.
[26] C. Théry, L. Zitvogel, S. Amigorena, Nat. Rev. Immunol. 2 (2002) 569–579.
[27] P.B. Devhare, R.B. Ray, Mol. Aspects Med. 60 (2018) 115–122.
[28] J.M. Pitt, G. Kroemer, L. Zitvogel, J. Clin. Invest. 126 (2016) 1139–1143.
[29] I.L. Colao, R. Corteling, D. Bracewell, et al., Trends Mol. Med. 24 (2018) 242–256.
[30] S. Fais, L. O'Driscoll, F.E. Borras, et al., ACS Nano 10 (2016) 3886–3899.
[31] L. Alvarez-Erviti, Y. Seow, H. Yin, et al., Nat. Biotechnol. 29 (2011) 341–345.
[32] W. Lv, Z. Han, Y. Li, et al., Chin. J. Chem. 39 (2021) 2107–2112.
[33] T. Wang, Y. Fu, S. Sun, et al., Chin. Chem. Lett. 34 (2023) 107508.
[34] B. György, M.E. Hung, X.O. Breakefield, et al., Annu. Rev. Pharmacol. Toxicol. 55 (2015) 439–464.
[35] D. Ha, N. Yang, V. Nadithe, Acta Pharm. Sin. B 6 (2016) 287–296.
[36] D. Rufino-Ramos, P.R. Albuquerque, V. Carmona, et al., J. Control. Release 262 (2017) 247–258.
[37] G. Jia, Y. Han, Y. An, et al., Biomaterials 178 (2018) 302–316.
[38] Y. Cao, T. Wu, K. Zhang, et al., ACS Nano 13 (2019) 1499–1510.
[39] S. Kamerkar, V.S. LeBleu, H. Sugimoto, et al., Nature 546 (2017) 498–503.
[40] Z. Mao, J. Chen, Y. Wang, et al., Nanoscale 14 (2022) 9474–9484.
[41] J. Zeng, Z. Li, H. Jiang, et al., Mater. Horiz. 8 (2021) 2964–3008.
[42] S. Azam, N. Hadi, N.U. Khan, et al., Toxicol. In Vitro 18 (2004) 555–561.
[43] M. Mochizuki, S. Yamazaki, K. Kano, et al., Biochim. Biophys. Acta 1569 (2002) 35–44.
[44] W.J. Xiu, S.Y. Gan, Q.R. Wen, et al., Research 2020 (2020) 9426453.
[45] S.Y. Xu, W. Yin, Y.L. Zhang, et al., Cancers 12 (2020) 372.
[46] Y. Wang, K. Huang, Z. Qin, et al., ACS Appl. Mater. Interfaces 14 (2022) 37291–37300.
[47] M.D. Nothling, H. Cao, T.G. McKenzie, et al., J. Am. Chem. Soc. 143 (2021) 286–293.
[48] J. Zeng, Z. Guo, Y. Wang, et al., Nano Res. 15 (2022) 4164–4174.
[49] J.K. Fredrickson, M.F. Romine, A.S. Beliaev, et al., Nat. Rev. Microbiol. 6 (2008) 592–603.
[50] P. Gwynne, Nature 495 (2013) S12–S13.
[51] P. Praveen, K. Loh, Bioresour. Technol. 206 (2016) 180–187.
[52] D. Davies, Nat. Rev. Drug Discov. 2 (2003) 114–122.
[53] Y. Zhao, X. Dai, X. Wei, et al., ACS Appl. Mater. Interfaces 10 (2018) 14426–14437.
[54] C. Angelo, D.C. Pierluigi, Z. Emanuela, et al., Microorganisms 4 (2016) 22.
[55] Y.S. Chen, P.V. Kamat, J. Am. Chem. Soc. 136 (2014) 6075.
[56] R. Jin, C. Zeng, M. Zhou, et al., Chem. Rev. 116 (2016) 10346–10413.
[57] W. Wei, Y. Lu, W. Chen, et al., J. Am. Chem. Soc. 133 (2011) 2060–2063.
[58] Y.P. Robert, J.F. Adam, Adv. Drug Deliv. Rev. 65 (2013) 1803–1815.
[59] J.H. Mohammad, M.F. Katharina, A.A. Ali, et al., Trends Biotechnol. 30 (2012) 499–511.
[60] R. Zhao, W. Kong, M. Sun, et al., ACS Appl. Mater. Interfaces 10 (2018) 17617–17629.
[61] Y. Xie, Y. Liu, J. Yang, et al., Angew. Chem. Int. Ed. 57 (2018) 3958–3962.
[62] H. Zhang, C. He, L. Shen, et al., Chin. Chem. Lett. 34 (2023) 108160.
[63] X. Zhang, X. Chen, J. Yang, et al., Adv. Funct. Mater. 26 (2016) 5958–5970.
[64] C. Chen, H. Yin, X. Chen, et al., Sci. Adv. 6 (2020) eaba0942.
[65] Q. Chen, C. Wang, X. Zhang, et al., Nat. Nanotechnol. 14 (2019) 89–97.
[66] J. Xu, J. Zhang, Z. Zhang, et al., Cell Death Dis. 12 (2021) 373.
[67] S. Rao, Y. Hu, P. Xie, et al., Bone Res. 6 (2018) 9.
[68] M.T. Wolf, C.L. Dearth, C.A. Ranallo, et al., Biomaterials 35 (2014) 6838–6849.